The Ser/Thr protein kinase PrkC imprints phenotypic memory in Bacillus anthracis spores by phosphorylating the glycolytic enzyme enolase

Richa Virmani, Andaleeb Sajid, Anshika Singhal, Mohita Gaur, Jayadev Joshi, Ankur Bothra, Richa Garg, Richa Misra, Vijay Pal Singh, Virginie Molle, et al.

HAL Id: hal-02282590

https://hal.science/hal-02282590

Submitted on 27 May 2021

The Ser/Thr protein kinase PrkC imprints phenotypic memory in *Bacillus anthracis* spores by phosphorylating the glycolytic enzyme enolase

Richa Virmani[‡§¶], Andaleeb Sajid[§], Anshika Singhal[§], Mohita Gaur[‡], Jayadev Joshi[§], Ankur Bothra[§], Richa Garg[§], Richa Misra[‡||], Vijay Pal Singh[§], Virginie Molle[**], Ajay K. Goel[‡‡], Archana Singh[§], Vipin C. Kalia[§§], Jung-Kul Lee[§§], Yasha Hasija[¶], Gunjan Arora[‡¶¶1], and Yogendra Singh[‡§2]

From the ‡Department of Zoology, University of Delhi, Delhi 110007, India, §Council of Scientific and Industrial Research (CSIR)–Institute of Genomics and Integrative Biology, Delhi 110007, India, ¶Delhi Technological University, Delhi 110042, India, ‡‡Defence Research and Development Establishment, Gwalior 474002, India, **Dynamique des Interactions Membranaires Normales et Pathologiques (DIMNP), CNRS, University of Montpellier, Montpellier 34000, France, ||Sri Venkateswara College, University of Delhi, Delhi 110021, India, §§Department of Chemical Engineering, Konkuk University, 1 Hwayang-Dong, Gwangjin-Gu, Seoul 05029, Republic of Korea, and ¶¶Laboratory of Immunogenetics, NIAID, National Institutes of Health, Rockville, Maryland 20851

Edited by Chris Whitfield

Bacillus anthracis is the causative agent of anthrax in humans, bovine, and other animals. *B. anthracis* pathogenesis requires differentiation of dormant spores into vegetative cells. The spores inherit cellular components as phenotypic memory from the parent cell, and this memory plays a critical role in facilitating the spores' revival. Because metabolism initiates at the beginning of spore germination, here we metabolically reprogrammed *B. anthracis* cells to understand the role of glycolytic enzymes in this process. We show that increased expression of enolase (Eno) in the sporulating mother cell decreases germination efficiency. Eno is phosphorylated by the conserved Ser/Thr protein kinase PrkC which decreases the catalytic activity of Eno. We found that phosphorylation also regulates Eno expression and localization, thereby controlling the overall spore germination process. Using MS analysis, we identified the sites of phosphorylation in Eno, and substitution(s) of selected phosphorylation sites helped establish the functional correlation between phosphorylation and Eno activity. We propose that PrkC-mediated regulation of Eno may help sporulating *B. anthracis* cells in adapting to nutrient deprivation. In summary, to the best of our knowledge, our study provides the first evidence that in sporulating *B. anthracis*, PrkC imprints phenotypic memory that facilitates the germination process.

Deciphering the role of metabolic enzymes that orchestrate morphogenic transition states in bacteria is a fundamental question. *Bacillus anthracis* is the causative agent of anthrax in humans, bovine, and other animals (1, 2). It is known to survive hostile environments by forming spores that remain quiescent and retain minimum metabolic activity (3, 4). As a pathogen, the success of *B. anthracis* depends on the spore's ability to develop into a growing vegetative cell. Under favorable conditions, spore metabolism is triggered to support energy needs and to develop into a fully functional cell (5). The metabolic checkpoints and energy reserves in the spore provide different stimuli at an early growth stage and ensure the completion of the developmental program. Therefore, the transformation of a dormant spore into a vegetative cell is a key step in the pathogenic cycle of *B. anthracis*. However, the molecular events leading to successful spore dormancy and later to germination remain to be fully elucidated.

During the process of germination, some spores disintegrate their protective structure and grow into vegetative cells (5). Sporulating cells carry a substantial set of macromolecules (including several proteins) through their journey from progenitor cell to spore (6). The role of these proteins remains largely unknown. This carryover of cellular components is termed "phenotypic memory" (7). The efficiency of spore germination has been shown to be determined by this phenotypic memory inherited from the parent cell (7, 8). In a recent study, the role of one such protein, alanine dehydrogenase, which controls alanine-induced outgrowth in cellular memory, was described (7). Because the protein cargo remains constant in the spore, these proteins decide the fate of the reviving spore depending on environmental conditions and sensory signaling molecules (9). There have been considerable efforts toward understanding the spore germination process and involvement of signaling mechanisms (10–12).

The link between metabolism and the spore revival process is not explored well. At the onset of germination, metabolism resumes without requiring new macromolecular synthesis (13). Reports in *Bacillus subtilis* have highlighted the essentiality and

interactions of glycolytic enzymes phosphofructokinase (Pfk),[3] phosphoglyceromutase (Pgm), and enolase (Eno) (14). Eno and Pgm play an essential role in both glycolysis and gluconeogenesis where Pgm reversibly converts 3-phosphoglyceric acid (3-PGA) to 2-PGA, and Eno catalyzes the penultimate step of glycolysis by conversion of 2-PGA to phosphoenolpyruvate (PEP), thus deciding the flux of pathway. Bacteria survive harsh conditions efficiently by keeping an alternate source of energy, 3-PGA, which is used during the early events of spore germination (15). A balanced ratio of 3-PGA and 2-PGA is maintained at the time of spore formation by keeping the spore metabolically dormant. Furthermore, the dehydrated, acidic core of spore diminishes the metabolic activity to maintain the 3-PGA reserve (16). Because spores of *Bacillus* sp. are known to hold significant levels of 3-PGA reserves, we decided to investigate the role of Eno in the spore germination process of *B. anthracis*. Previous studies have shown that an Eno deletion-mutant strain was defective in sporulation, whereas its inhibition led to a lag in ATP production during germination, thus uncovering a role for Eno in the bacterial life cycle (17, 18). Besides this, Eno is a component of the adsorbed anthrax vaccine and has been indicated in helping bacteria evade the innate immune cells by binding to host plasminogen (19, 20).

In this study, we address the role of Eno in spore germination. Our results show that Eno acts as an intrinsic memory controller that influences the germination process and is regulated by the Ser/Thr protein kinase PrkC.

Results and discussion

B. anthracis Eno influences spore germination

To decipher the contribution of some key metabolic enzymes in spore germination, we cloned and expressed the glycolytic pathway genes *pgk*, *pgm*, and *eno* that are important for maintaining the 3-PGA reserve. The *B. anthracis* Sterne (Bas) strains overexpressing Pgk, Pgm, and Eno were analyzed for their sporulation and germination efficiencies. As shown in Fig. 1*A*, an increase in the expression of either glycolytic protein led to a decrease in sporulation efficiency. For germination efficiency, there was an ~75% decrease in Eno-overexpressing spores, whereas spores overexpressing Pgk and Pgm showed only about 20 and 40% decreases, respectively (Fig. 1*B*). To assess the levels of Eno in the overexpression strain, we generated Eno-specific polyclonal antibodies in mice (Fig. S1). Immunoblotting with these antibodies showed that the expression of Eno was increased by ~1.5-fold in the recombinant strain as compared with parent strain (Fig. S2).

Eno expression is reduced in B. anthracis spores

Our results suggest that overexpression of Eno causes a decrease in spore germination. Therefore, we decided to check the intrinsic regulation of Eno expression in spores as well as in vegetative cells. Using Eno-specific polyclonal antibodies, we
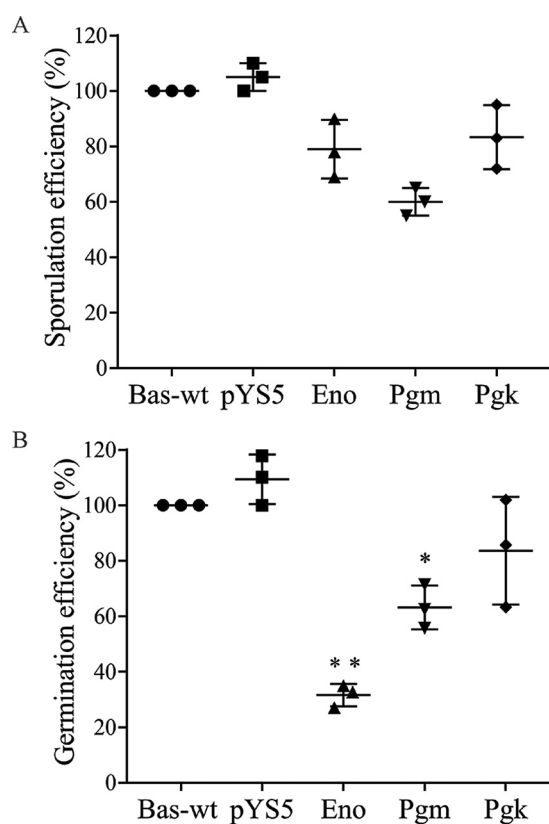

Figure 1. Role of Eno in spore germination. The bacterial strains Bas-wt or Bas overexpressing the desired gene (Eno, Pgm, Pgk, and pYS5 vector control) were used for spore formation followed by the addition of nutrient-rich medium for germination. Sporulation (*A*) and germination (*B*) efficiencies were calculated considering the efficiency of Bas-wt as 100% and plotted using GraphPad Prism. *Error bars* represent S.D. of three independent experiments. *, $p \leq 0.05$; **, $p \leq 0.01$ as determined by two-tailed unpaired Student's *t* test.

determined the expression of Eno in whole-cell lysates at different stages of the *B. anthracis* lifecycle. Immunoblotting with anti-Eno antibody detected a specific band at ~45 kDa corresponding to the molecular mass of Eno. After quantification of band intensities, differential expression of Eno was observed in several growth stages relative to early log phase where the maximum expression was observed (Fig. 2). The expression of Eno consistently decreased in the later growth stages (log phase, late log phase, and stationary phase) until in a spore-forming stage where only 30% of the protein remained with respect to early log phase. Because spores have lower levels of Eno as compared with vegetative cells and overexpression of Eno leads to reduced fitness of the Bas strain during spore germination, there seems to be a decisive role of Eno in germination.

Eno is phosphorylated in vitro by the B. anthracis Ser/Thr protein kinase PrkC

Signaling mechanisms regulate the transition of *B. anthracis* from dormancy to vegetative state (21, 22). Interestingly, there is a growing body of evidence supporting the notion that PrkC could play an important role in the spore's exit from dormancy (12, 23, 24). In our previous studies, we found that glycolytic enzymes are subjected to regulation by phosphorylation (25, 26). Large-scale phosphoproteome analysis in *B. subtilis* also

---

[3] The abbreviations used are: Pfk, phosphofructokinase; pgk, phosphoglycerate kinase; Pgm, phosphoglyceromutase; Eno, enolase; PGA, phosphoglyceric acid; PEP, phosphoenolpyruvate; Bas, *B. anthracis* Sterne; Eno-P, phosphorylated Eno; Eno-UP, unphosphorylated Eno; PA, protective antigen; cfu, colony-forming unit.
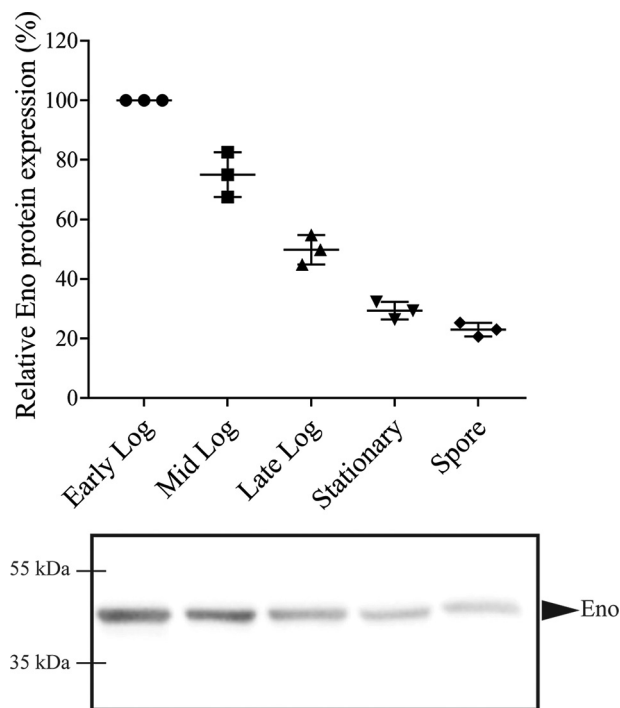
Figure 2. Decreased expression of Eno in *B. anthracis* spores. Expression of Eno was analyzed by immunoblotting of lysates of different growth phases (early log ($OD_{600} = 0.2$–0.3), log phase ($OD_{600} = 0.8$–1.0), late log ($OD_{600} = 1.5$–1.7), and stationary phase ($OD_{600} > 2.2$)) and spores with anti-Eno antibody. The histogram (*upper panel*) shows relative expression of Eno, which was calculated taking the expression of Eno in early log phase as 100% in the corresponding representative blot image (*lower panel*). *Error bars* represent S.D. of three independent experiments.

indicates phosphorylation of Eno, which is a close homolog of *B. anthracis* Eno (~80% sequence similarity) (27). Additionally, in our previous study, comparison of phosphoproteomic analyses of *B. anthracis* WT (Bas-wt) and *prkC* deletion mutant (BasΔprkC) identified phosphorylated isoforms of Eno (28). Therefore, we hypothesized that Eno could be regulated by PrkC-mediated phosphorylation, and this regulation might be important for *B. anthracis* morphogenesis.

To address this hypothesis, *in vitro* kinase assays were performed using recombinant PrkC and Eno with [γ-^{32}P]ATP. As shown in Fig. 3*A*, Eno was found to be phosphorylated by PrkC. No phosphotransfer was observed when Eno was incubated alone or with the Ser/Thr phosphatase PrpC. Phosphotransfer analysis using *in vitro* kinase assay and two-dimensional gel electrophoresis indicated phosphorylation of Eno at early time points (Fig. 3, *B–D*). Thus, these assays confirmed that Eno is a substrate of PrkC. Subsequently, the phosphorylation of Eno was also confirmed *in vivo* using coexpression with PrkC and PrpC in *Escherichia coli*. Eno was found to be phosphorylated when coexpressed with PrkC (phosphorylated Eno (Eno-P)), whereas no phosphorylation was observed when coexpressed with PrpC (unphosphorylated Eno (Eno-UP)) as confirmed by Pro-Q Diamond phosphorylation-specific staining (Fig. 3*E*). Eno-P isolated from cells metabolically labeled with [^{32}P]orthophosphoric acid showed a ^{32}P-labeled Eno demonstrating PrkC-specific phosphorylation under native conditions in *E. coli* (Fig. 3*F*).

Eno is phosphorylated on serine and threonine residues

To identify the residues in Eno that are phosphorylated by PrkC, purified Eno-P and Eno-UP proteins were subjected to MS (Fig. S3). We found nine phosphorylated serine and threonine residues in Eno-P, whereas no phosphorylated residues were identified in Eno-UP. To identify the location of phosphorylation sites in Eno, we generated a homology model of *B. anthracis* Eno using the crystal structure of *B. subtilis* Eno (Protein Data Bank (PDB) code 4A3R) (29). Fig. 4*A* shows the Bas Eno homology model with the phosphorylation sites marked. Three phosphorylated residues (Ser^{336}, Thr^{363}, and Ser^{367}) were localized in the C-terminal hydrophobic region, whereas the remaining six residues were present at the protein surface (Fig. 4*A*). Among these sites, Ser^{367} was highly conserved among the Eno homologs and was found to be present in the flexible loop responsible for catalysis, as identified by multiple sequence alignment of Eno and its homologs (Fig. S4). Previously, Eno Ser^{367} was also identified as a phosphorylated residue in the spore phosphoproteome of *B. subtilis* (27). Further structural analysis of the three C-terminal residues indicated that Ser^{367} could interact with the catalytic site residues Lys^{340} and Ile^{339} (Fig. 4*B*), whereas Thr^{363} and Ser^{336} were present on the parallel and antiparallel strands, stabilizing the structure of the protein (Fig. 4*C*).

To determine the role of individual phosphorylation sites, we chose to study the three C-terminal residues located in the hydrophobic pocket. These residues were mutated to generate single mutants Eno^{T363A}, Eno^{S336A}, and Eno^{S367A}; a double mutant, Eno$^{S336A/T363A}$; and a triple mutant, Eno$^{S336A/T363A/S367A}$. Equal amounts of Eno and its mutant derivatives were used in an *in vitro* kinase assay with PrkC. Quantification of phosphorylation levels indicated a significant decrease in signal for all the single Eno mutants, whereas the double mutant Eno$^{S336A/T363A}$ showed a >60% loss in phosphorylation levels (Fig. 4*D*). In the triple mutant (Eno$^{S336A/T363A/S367A}$), there was a significant loss (>80%) in phosphorylation (Fig. 4*E*), showing that Ser^{336}, Thr^{363}, and Ser^{367} were important phosphorylation sites.

The role of these three residues in regulating the enzyme activity was also analyzed. In glycolysis, Eno catalyzes the penultimate step by converting 2-PGA to PEP. We evaluated the phosphorylation-mediated variations on the activity of Eno by using a kit-based colorimetric assay that measures the formation of an intermediate product during this conversion. As shown in Fig. 4*F*, a considerable loss (40–50%) in the activity of Eno^{S336A} and Eno^{S367A} mutants was observed, whereas Eno^{T363A} exhibited an increase in activity. Furthermore, the triple mutant showed a ~40% decrease in the overall protein activity as compared with Eno-wt (Fig. 4*G*).

To understand the effect of mutations on the structural integrity of Eno, we performed circular dichroism (CD) spectroscopy using Eno purified from *E. coli* (Eno-wt), Eno-P (Eno coexpressed with PrkC), Eno-UP (Eno coexpressed with PrpC), and the triple mutant Eno$^{S336A/T363A/S367A}$. To our surprise, all four samples showed a similar α-helix and β-sheet composition, suggesting that the mutations as well as phosphorylation
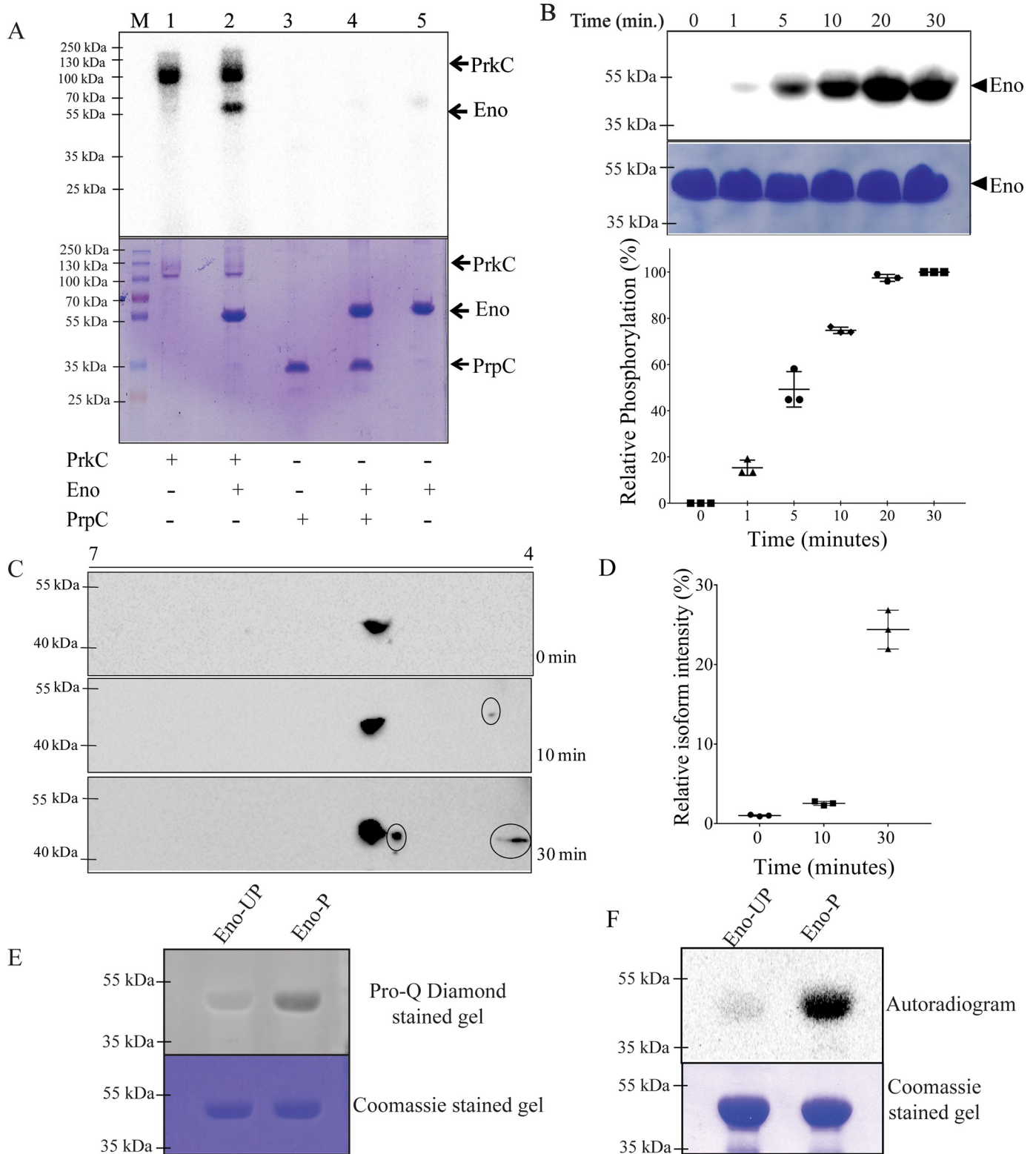
Figure 3. Eno is phosphorylated by PrkC *in vitro*. *A*, autoradiogram (*upper panel*) showing phosphorylation of recombinant Eno (5 μg) by PrkC (1 μg). PrpC (1 μg) and Eno alone were used as negative controls. The corresponding SDS-PAGE is shown (*lower panel*). *Lane M*, molecular mass markers. *B*, autoradiogram showing time-dependent phosphorylation of Eno (*top panel*) that was normalized to protein amounts and plotted using GraphPad Prism (*lower panel*). The intensity of phosphorylation of protein bands was calculated using QuantityOne software. Eno phosphorylation after 30 min was taken as 100% (signal saturation), and relative phosphorylation was calculated. The *error bars* show S.D. of three independent experiments. *C* and *D*, time-dependent phosphorylation of Eno by PrkC using cold ATP. Isoforms were resolved by 2D gel electrophoresis, and subsequent blots were probed with anti-Eno antibodies to determine the stoichiometry of Eno phosphorylation at different time points. Multiple species (*encircled*) were observed after 30 min of the reaction as compared with 0 and 10 min, and their relative intensity was calculated and plotted using GraphPad Prism. *E* and *F*, His-Eno purified from *E. coli* cells expressing Eno with PrkC (Eno-P) or PrpC (Eno-UP) were resolved by SDS-PAGE and stained with Pro-Q Diamond followed by analysis using a Typhoon imager (*E*). *E. coli* cells overexpressing Eno-P or Eno-UP were subjected to metabolic labeling using [^{32}P]orthophosphoric acid (*F*). In both panels, Eno-P was found to be phosphorylated, whereas no phosphorylation was observed on Eno-UP.

A

B

C

D

E

F

G
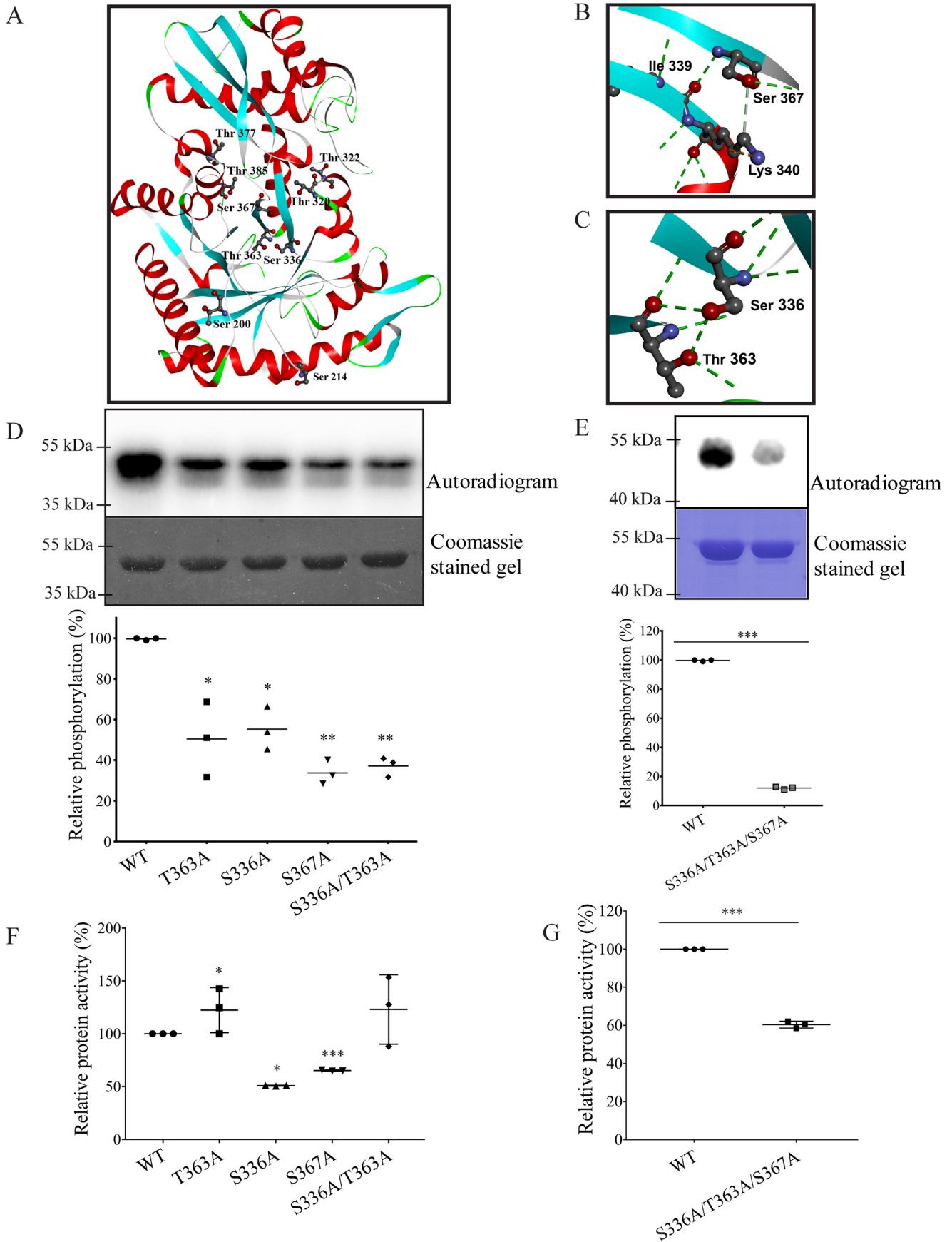
Table 1
Kinetic parameters of circular dichroism analysis

Parameters	Eno-wt	Eno$^{S336A/T363A/S367A}$	Eno-P	Eno-UP
α-Helix (%)	71.56	69.91	69.84	70.85
β-Strand (%)	5.06	5.13	5.18	4.88

do not affect the secondary structure of the protein and maintain overall conformation (Table 1).

Previous studies on Eno structure from diverse species have shown that Ser^{367} is a part of a flexible loop as mentioned earlier (30). This flexible loop is involved in binding to 2-PGA and subsequent conformational change. Additionally, we found this loop to be conserved in Eno from different species (Fig. S4). Therefore, we speculate that this flexibility of the loop and associated conformational change in the absence of substrate might allow the residue to become phosphorylated by the kinase (31).

Eno is phosphorylated in B. anthracis vegetative cells and spores

We next investigated the *in vivo* phosphorylation status of Eno. We overexpressed Eno with a C-terminal polyhistidine tag in Bas-wt (Bas Eno) and BasΔprkC (BasΔprkC Eno) Sterne strains. Purified proteins from respective strains were subjected to immunoblotting using anti-pSer and anti-pThr antibodies. Eno-P (coexpressed with PrkC) was used as a positive control, and *E. coli* Eno (not coexpressed with PrkC) was used as a negative control. pSer- and pThr-specific antibodies recognized Eno purified from Bas-wt, whereas the phosphorylation signal was significantly reduced, although not completely absent, in the BasΔprkC strain (Fig. 5, *A and B*). This result indicates that Eno is predominantly phosphorylated by PrkC *in vivo* but may also be phosphorylated by other kinases in the absence of PrkC.

Furthermore, we analyzed the stoichiometry of *in vivo* phosphorylation of Eno by resolving the phosphorylated and unphosphorylated isoforms on 2D gel electrophoresis. Whole-cell protein extracts from Bas-wt and BasΔprkC were subjected to electrophoresis followed by immunoblotting with anti-Eno antibody. Four Eno isoforms were observed in BasΔprkC cells (Fig. 5C). However, in Bas-wt cells, we identified seven Eno isoforms among which four were present at a pI similar to that in the BasΔprkC strain (pI 4.5–5.0), whereas the remaining three isoforms migrated at acidic pI range (toward 4.0; Fig. 5C), thus confirming PrkC-specific phosphorylation of Eno in vegetative cells.

Next, we investigated whether Eno was phosphorylated in spores. We overexpressed and purified Eno from *B. anthracis* spore lysate (Eno Bas Spore) followed by immunoblotting with anti-pThr antibody. Eno phosphorylation was detected in spores despite its low expression (Fig. 5D). The phosphorylation was also confirmed by using anti-pSer antibodies (Fig. S5).

These results show that Eno is regulated by PrkC-mediated phosphorylation in spores of *B. anthracis*, confirming its role in spore germination.

Phosphorylation decreases catalytic activity and Mg^{2+} cofactor affinity of Eno

After establishing that Eno is a substrate of PrkC, we investigated the effect of phosphorylation on Eno activity. In the activity assay, Eno-P was found to be ~60% less active than Eno-UP, suggesting that phosphorylation causes a decrease in the activity of Eno (Fig. 6A).

Interestingly, spores contain high concentrations of divalent cations such as Ca^{2+}, Mg^{2+}, and Mn^{2+} to keep themselves dehydrated, thus maintaining a low metabolic profile (32, 33). As Eno is a metalloenzyme requiring Mg^{2+} as a cofactor (34), we investigated whether phosphorylation had an impact on Eno–Mg^{2+} interaction. Eno-P and Eno-UP (coexpressed with PrkC and PrpC, respectively) were used to study the phosphorylation-mediated regulation of the Eno–Mg^{2+} interaction. A fluorimetry-based method was used to measure variations in the intrinsic tryptophan fluorescence of Eno upon addition of MgCl$_2$ (35). We observed that Eno–Mg^{2+} complex formation was correlated with an enhancement of tryptophan fluorescence intensity. Our data showed that fluorescence of Eno-UP with Mg^{2+} was higher than that of Eno-P, indicating a negative effect of phosphorylation on metal binding (Fig. 6B). Different concentrations of Mg^{2+} were titrated with Eno-UP or Eno-P, and the binding constant (K_a) was calculated. For Eno-UP, the K_a was higher (0.254 ± 0.01 M) than the K_a for Eno-P (0.181 ± 0.03 M). Hence, these results show that Eno phosphorylation reduces Mg^{2+} binding affinity, which is in agreement with the decreased activity of phosphorylated Eno.

PrkC is involved in the regulation of Eno expression in spores

We further analyzed the effect of PrkC on Eno expression in spores by comparing the protein levels of Eno in spores of Bas-wt and BasΔprkC Sterne strains (Fig. 7A) as well as during exponential growth (Fig. 7B). Our results showed 2–3-fold higher protein levels of Eno in BasΔprkC spores compared with Bas-wt spores, whereas the expression was similar in both strains during the exponential phase (Figs. 7 and S6). Thus, Eno protein levels might be regulated by PrkC. These results could in part explain the compromised virulence phenotype of the PrkC-null mutant as observed in earlier studies (36). However, it remains to be determined whether this PrkC-dependent regulation is direct or indirect. It could be hypothesized that PrkC phosphorylates a yet to be discovered transcription factor that regulates the expression of Eno. Such regulation could occur

Figure 4. Mapping of the Eno phosphorylation sites. *A*, cartoon representation of the homology model of Eno from *B. anthracis*, generated using coordinates of the crystal structure of Eno from *B. subtilis* (PDB code 4A3R). Helices are colored *red*, and sheets are colored *cyan*. The phosphorylation sites of Eno-P, as identified by MS, are indicated using the *ball-and-stick* model and are labeled. Six Thr residues (Thr^{200}, Thr^{320}, Thr^{322}, Thr^{363}, Thr^{377}, and Thr^{385}) and three Ser residues (Ser^{214}, Ser^{336}, and Ser^{367}) were identified. *B* and *C*, residues Ser^{336}, Ser^{367}, and Thr^{363}, which are evaluated in *D* and *F*, are shown. *Green dashed lines* indicate H-bonds. *D* and *E*, nonphosphorylatable mutants of Eno (Ser/Thr to Ala) were assessed for their phosphorylation extent relative to the native Eno (100%). The *in vitro* kinase assay of PrkC with mutants was analyzed by autoradiogram (*upper panel*) and quantified by QuantityOne (*lower panel*). *F* and *G*, relative activity of Eno mutants with respect to the native Eno (100%). Native Eno is named as WT, and mutants are named with respective mutation sites. All experiments were performed thrice, and *error bars* represent S.E. of three independent values. *, $p \leq 0.05$; **, $p \leq 0.01$; ***, $p \leq 0.001$ as determined by two-tailed unpaired Student's *t* test.
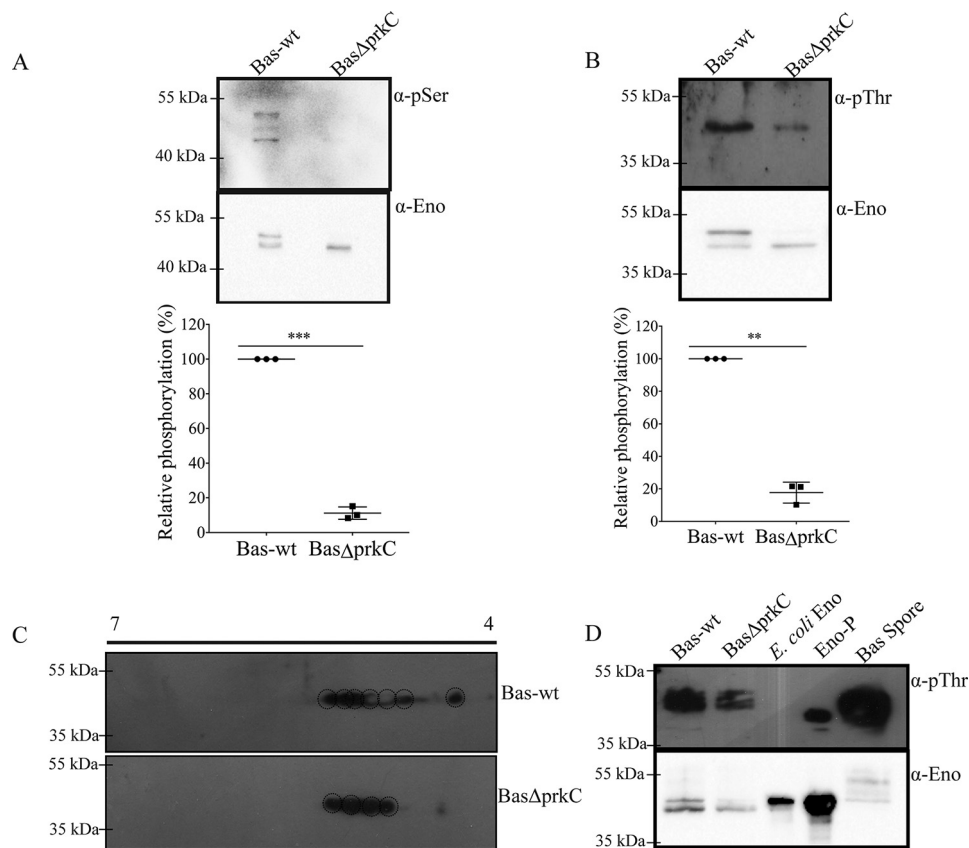
Figure 5. Phosphorylation of Eno in *B. anthracis* vegetative cells and spores. *A*, *B*, and *D*, Bas Eno was overexpressed and purified from Bas-wt, BasΔprkC, and Bas-wt spores. The protein was resolved using SDS-PAGE and probed with anti-phosphoserine and anti-phosphothreonine antibodies. The blots were normalized by reprobing the blot with anti-Eno antibody. *Error bars* represent S.D. of three independent experiments. *C*, the cell lysates of Bas-wt and BasΔprkC strain were subjected to 2D gel electrophoresis and probed with anti-Eno antibodies to determine the stoichiometry of native Eno phosphorylation. Multiple species were observed in Bas-wt lysates as compared with BasΔprkC, which shows Eno phosphorylation by PrkC. **, $p \leq 0.01$; ***, $p \leq 0.001$ as determined by two-tailed unpaired Student's *t* test.

upon a signal received by PrkC at the onset of sporulation to trigger Eno down-regulation.

Eno phosphorylation status does not regulate its secretion but may affect its cellular localization

Surface-exposed signaling proteins like PrkC might be involved in maintaining the cellular dynamics during morphogenesis by modifying the activities and localization of metabolic enzymes to fulfill cellular requirements. Therefore, we examined whether the phosphorylation status of Eno could be linked to its cellular localization. To determine the localization of Eno within the vegetative cells, we probed the native protein in Bas-wt cells in exponential phase by anti-Eno antibodies using immuno-EM. Eno was found to be localized at the cell membrane and cytoplasm (Figs. 8, *A* and *B*, and S7). Subsequently, we compared the localization of Eno in BasΔprkC and *prkC*-complemented strains at the exponential stage and noticed variability in Eno localization patterns among all three strains. Eno was found to be predominantly localized on the cell membrane in the BasΔprkC strain as compared with the Bas-wt and *prkC*-complemented strains (Fig. 8*B*), indicating that the unphosphorylated isoform preferentially localizes at the membrane in vegetative cells.

In *B. subtilis*, Eno is known to be secreted via the nonclassical secretion pathway through a membrane-embedded hydropho-

bic domain (37, 38). We checked whether Eno secretion could also be impacted upon phosphorylation. So, culture supernatants and cell lysates of the Bas-wt and BasΔprkC cells grown to the late exponential phase were subjected to immunoblotting with anti-Eno antibodies. As a control, we used a very well-known secretory protein from *B. anthracis*, the protective antigen (PA), which also forms part of the anthrax vaccine. The supernatant fraction was probed with the polyclonal antibody to PA to confirm that the supernatant contained the secreted proteins. Immunoblotting showed that *B. anthracis* Eno is secreted from the cell, but secretion was independent of its phosphorylation status (Fig. 8*C*). Thus, we conclude that PrkC affected the localization of Eno but not its secretion.

Conclusions

Development of spore to a vegetative cell requires a shift in metabolism. During spore formation, bacteria down-regulate their metabolism by halting transcriptional and translational machinery and storing energy reserves. At the beginning of germination, a spore requires substantial metabolic supplements. PrkC is known to sense germination cues from the environment and helps in regulating translation and metabolism during the spore germination. One of the primary questions in cellular development is how the metabolic machinery switches from dormancy during sporulation to exponential growth dur-
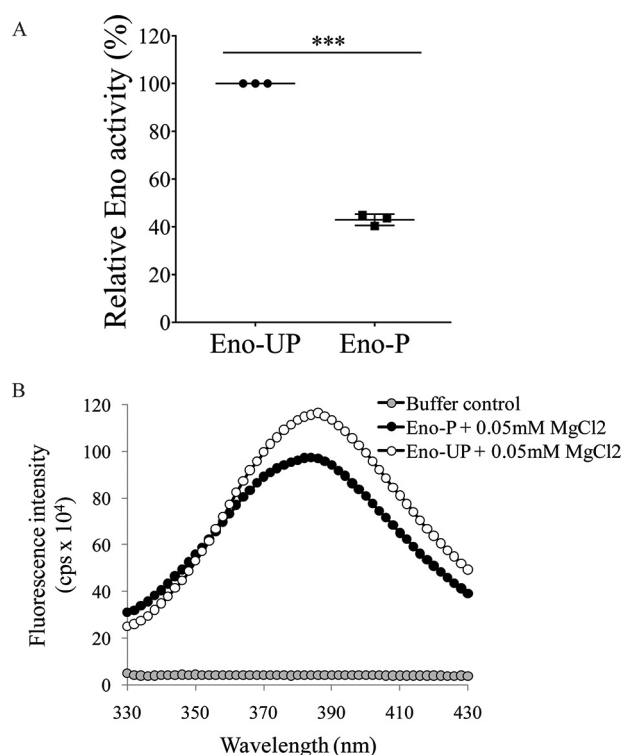
Figure 6. Effect of phosphorylation on Eno activity. *A*, Histogram showing the comparative activity of Eno-P and Eno-UP. Phosphorylated and unphosphorylated forms were compared in identical conditions. The activity was calculated taking Eno-UP as 100%. The experiments were performed thrice and the *error bars* show S.D. of three values. *B*, the interaction of Eno-P and Eno-UP (1 μM each) with MgCl$_2$ (0.05 mM) was recorded from 330 to 430 nm after excitation at 280 nm. ***, $p \leq 0.001$ as determined by two-tailed unpaired Student's t test.
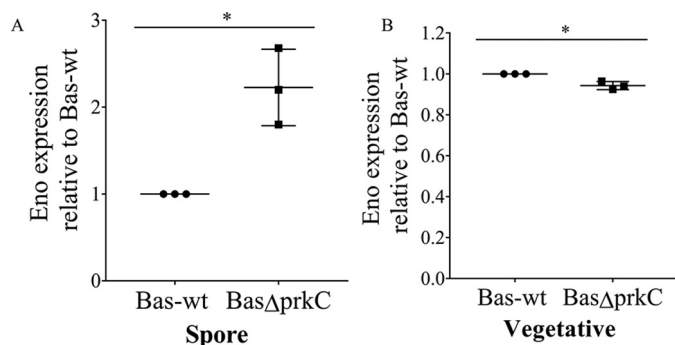

Figure 7. Relative expression of Eno. Eno expression was analyzed by comparing the spore lysates (*A*) and vegetative cell lysates (exponential phase) (*B*) of Bas-wt and *prkC* deletion (BasΔprkC) strains. The expression level was calculated using the Western blots (Fig. S6) by Fiji-ImageJ and represents the mean with *error bars* showing S.D. of three independent values. *, $p \leq 0.05$ as determined by two-tailed unpaired Student's t test.

ing germination. Phenotypic memory, which is a carryover of cellular material from the mother cell to the spore, is key to germination. A critical step in this developmental program is the regulation of glycolytic enzymes that store energy reserves and balance metabolic needs when germination begins. We studied the expression of three glycolytic enzymes and identified Eno as a metabolic switch that holds the key to germination and contributes to phenotypic memory. Our results further identified PrkC to augment the germination process by maintaining Eno quantity, localization, and its enzymatic activity (Fig. 9).

In conclusion, our results provide evidence of Eno regulation by phosphorylation and its involvement in the process of germination of *B. anthracis* spores. Our study elucidates the phosphorylation of Eno and identifies its regulation by PrkC. The role of PrkC has been previously discussed in spore germination (12). Our results show that during sporulation PrkC initiates imprinting phenotypic memory by modifying the metabolic protein Eno. This imprinted memory helps *B. anthracis* to survive the nutritional shift and helps in spore germination.

Experimental procedures

Bacterial strains and growth conditions

E. coli strains DH5α (Novagen) and BL21-DE3 (Agilent) were used for cloning and expression of recombinant proteins, respectively. *E. coli* cells were grown and maintained with constant shaking (200 rpm) at 37 °C in LB broth supplemented with 100 μg/ml ampicillin or 25 μg/ml chloramphenicol for the coexpression system. Bas-wt, PrkC deletion strain (BasΔprkC) and *prkC*-complemented strains (BasΔprkC complement) (12) were grown in LB medium supplemented with antibiotics as required. LB agar was used as the solid medium for culturing both *E. coli* and *B. anthracis* in the presence of selective antibiotics.

Cloning and mutagenesis of B. anthracis genes

Cloning and mutagenesis were performed according to the standard molecular biology procedures described earlier using *B. anthracis* Sterne strain genomic DNA (39, 40). The coding sequences of *eno* (Bas4985), *pgm* (Bas4986), and *pgk* (Bas4988) from *B. anthracis* were amplified by PCR using primers containing SpeI and BamHI restriction sites with six-histidine repeat sequences in the reverse primer (Table S1). The resulting PCR product was cloned into *E. coli*/*B. anthracis* shuttle vector pYS5. Clones were then confirmed with restriction digestion and DNA sequencing (SciGenome). The confirmed plasmid was electroporated in Bas-wt or BasΔprkC strain using BTX Electro Cell Manipulator 600. For cloning and expression in *E. coli*, *eno* was amplified by PCR using primers containing BamHI and XhoI restriction sites. The resulting PCR product was cloned in pPro-Ex-HTc. To generate the site-specific mutants of Eno, site-directed mutagenesis was performed using the QuikChange® XL Site-Directed Mutagenesis kit (Agilent).

Expression and purification of recombinant B. anthracis proteins

The recombinant His$_6$-tagged fusion proteins were overexpressed and purified from *E. coli* and *B. anthracis* as described previously (28). *E. coli* BL21-DE3 strains harboring plasmid pACYC-PrkC or pACYC-PrpC were cotransformed with Bas4985 (*eno*)–containing plasmid (pProEx-HTc) to overexpress and purify Eno-P or Eno-UP, respectively. The phosphorylation status was checked by staining with Pro-Q Diamond phospho-specific stain (Molecular Probes, Life Technologies) according to the manufacturer's instructions. The protein amounts were checked by SYPRO Ruby protein gel stain (Molecular Probes, Life Technologies) and Coomassie Brilliant Blue stain.
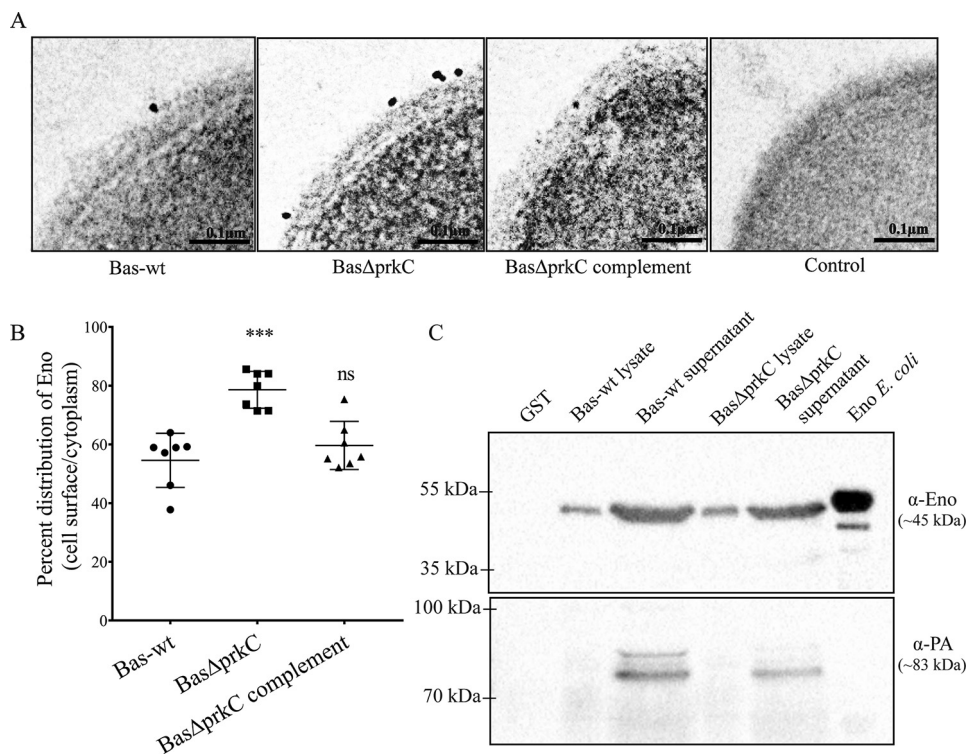
Figure 8. Localization and secretion of Eno in *B. anthracis*. *A* and *B*, quantitative analysis of surface localization of Eno in Bas-wt, BasΔprkC, and BasΔprkC complement strains using anti-Eno (*A*) by counting the gold particles on the bacterial cell surface (*n* = 7) using Fiji-ImageJ. *Error bars* represent S.D. of seven values. Preimmune serum was used as a negative control. A section is shown for immuno-EM; the full image is also provided in Fig. S7. *C*, lysates and the secretory fraction from Bas-wt and BasΔprkC were subjected to immunoblotting using anti-Eno antibody (*upper panel*) and normalized by reprobing with anti-PA (for normalization). ***, $p \leq 0.001$; *ns*, not significant as determined by two-tailed unpaired Student's *t* test.

Sporulation and germination efficiency

Spores were prepared as described in the previous study (41). Different dilutions of heat-treated and nontreated spores were plated on LB agar, and cfu were counted. The sporulation efficiency was calculated as cfu per ml (heat-treated)/cfu per ml (nontreated) and compared with respect to Bas-wt (taken as 100%) (42). For germination efficiency, spores were diluted to an OD_{600} of 1 and heat-treated at 70 °C for 30 min (43). The heat-treated spores were serially diluted in deionized water, plated on LB agar (without antibiotics), and incubated at 37 °C overnight. cfu were counted, and Bas-wt spore cfu were taken as 100%. Statistical analysis was performed using parametric *t* test.

Eno activity assay

The activity of His_6-tagged Eno-UP and Eno-P (1 μg) was measured using an Eno colorimetric activity assay kit according to the manufacturer's protocol (Biovision). Eno catalyzes the conversion of 2-PGA to PEP. The intermediate product formed reacts with a peroxide substrate to generate color (OD_{570}) at 25 °C proportional to the Eno activity. A standard curve was generated with different dilutions of H_2O_2, and Eno activity was calculated using the following formula.

$$\text{Enolase activity} = \frac{B \times \text{Sample dilution factor}}{(\text{Reaction time}) \times V} \quad \text{(Eq. 1)}$$

Where *B* is the amount (nmol) of H_2O_2 generated between T_{initial} and T_{final} reaction: Reaction time = $T_{\text{final}} - T_{\text{initial}}$ (min). *V* is the sample volume (ml) added to the well.

In vitro kinase assay

PrkC (1 μg) was used for *in vitro* kinase assay with Eno and its mutants in kinase buffer (20 mM HEPES, pH 7.2, 10 mM $MgCl_2$, and 10 mM $MnCl_2$) containing 2 μCi of [γ-^{32}P]ATP (BRIT, Hyderabad, India) at 25 °C for 30 min as described previously (25).

Metabolic labeling

E. coli BL21-DE3 transformants harboring either pACYC-PrkC:Eno or pACYC-PrpC:Eno were used for metabolic labeling using [γ-^{32}P]orthophosphoric acid as described previously (44). Extracted samples were analyzed by autoradiography using a Personal Molecular Imager (PMI, Bio-Rad).

Mass spectrometry analysis

Samples were resolved by SDS-PAGE and trypsinized to prepare peptide mixtures for mass spectrometric analysis (45). Peptides were separated and measured by LC–electrospray ionization–MS using the Easy-nLCII HPLC system (Thermo Fisher Scientific) coupled directly to an LTQ Orbitrap Velos™ mass spectrometer (Thermo Fisher Scientific). Proteins were identified by searching all MS/MS spectra against a forward–reverse database that was composed of all protein sequences of *B. anthracis* Sterne and common contaminants using Sorcer-er™-SEQUEST (version v.27, rev.11, Thermo Fisher Scientific) in conjunction with Scaffold (version 3 00 06, Proteome Software Inc., Portland, OR).
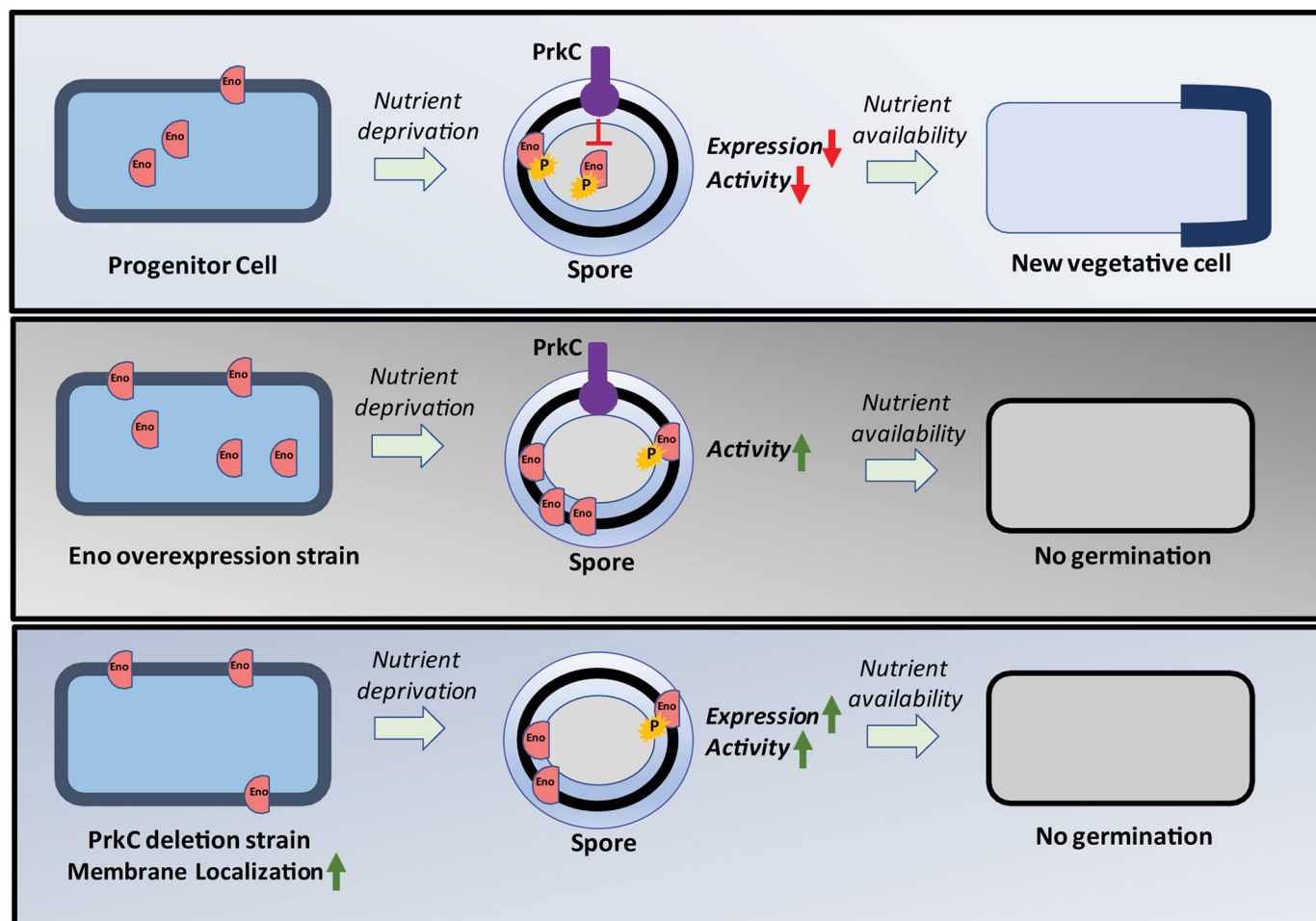
Figure 9. Proposed model illustrating PrkC and Eno interactions. The interactions and their impact on bacterial spore germination are shown in native *B. anthracis*, *B. anthracis* overexpressing Eno, and *B. anthracis* PrkC-deficient strains. *Top panel*, native Eno expression. In Bas-wt cells, there is a basal-level expression of Eno in vegetative cells that is carried over in the spores. The expression and activity are kept low by PrkC through phosphorylation so that the spores can germinate effectively. *Middle panel*, Eno overexpression strain. The expression is raised to 1.5-fold in this strain with subsequent activation in the spore leading to spore germination defect. *Bottom panel*, PrkC-deficient strain. Membrane-localized unphosphorylated Eno is carried over in spores with increased expression and activity leading to spore germination defect.

Immuno-EM

Bas-wt, kinase-deletion mutant (BasΔprkC), and the complemented strain (BasΔprkC complement) were grown at 37 °C to mid-log phase and harvested. The cells were fixed in 2% paraformaldehyde and 0.05% glutaraldehyde dissolved in 0.1 M sodium phosphate buffer (PB), pH 7.4, for 2 h and then washed three times with PB. The cells were then resuspended in 2% agar and harvested again. The cell pellets were immersed in 30% sucrose (w/v) overnight at 4 °C and subjected to immunolabeling as described previously (46) using a 1:10 dilution of anti-Eno antibodies and preimmune serum as a control. Ultrathin sections (70 nm thick) were cut on an RMC ultramicrotome, stained with 1% uranyl acetate, and imaged in a Tecnai G2 20 twin (FEI) transmission electron microscope. Cell-surface enolase expression was normalized with cytosolic expression using Fiji-ImageJ and plotted using GraphPad Prism.

Magnesium binding assay

The Eno-UP and Eno-P forms of Eno were used in interaction studies with $MgCl_2$. The reaction was initiated by the addition of the each of the proteins (1 μM) to fluorescence assay buffer, buffer F (1 mM PEP (Sigma), 0.1 M HEPES, pH 7, and 7.7 mM KCl) with $MgCl_2$ (0.05 mM). A buffer containing PEP, HEPES, and KCl served as a control. The emission spectra were recorded from 310 to 430 nm after excitation at 280 nm (Fluoromax-3 spectrofluorimeter, Jobin Yvon Horiba) with an integration time of 1s. The association of $MgCl_2$ with Eno was measured by mixing increasing concentrations of $MgCl_2$ (0.05–10 mM) with a 1 μM concentration of Eno (Eno-P and Eno-UP) in buffer F at 25 °C. The experiment was performed by monitoring the fluorescence change over time (35).

Enzyme-linked immunosorbent assay (ELISA)

An indirect ELISA was performed as described earlier with some modifications (47). Briefly, His_6-tagged Eno (100 ng/well) was dissolved in a coating buffer (carbonate-bicarbonate buffer, pH 9.6) and adsorbed on the surface of a 96-well ELISA plate (Maxisorb, Nunc) for 16 h at 4 °C. The test serum was serially diluted (1% in phosphate-buffered saline (PBS)) and added to each well to be kept for 1 h at 37 °C. Preimmune serum was used as a control. The experiment was done in triplicates, and the antibody titer was expressed as the reciprocal of the end-point dilution.

ASBMB

J. Biol. Chem. (2019) 294(22) 8930–8941 **8939**

Antibody generation and Western blotting

B. anthracis Eno (Bas4985) expressed in *E. coli* with a His$_6$ tag was purified with up to 98% homogeneity (as per SDS-PAGE analysis). The affinity-purified protein was dialyzed against PBS and confirmed to be endotoxin-free using a kit-based assay (Pierce). The protein was then used to immunize a group of Rabbit and BALB/c mice ($n = 3$) first in combination with Freund's complete adjuvant and subsequently Freund's incomplete adjuvant. After three booster doses (2 weeks apart), the animals were bled, and the isolated serum was analyzed using an indirect ELISA, which showed an efficient titer against Eno. The specificity of the Western blots was determined by probing *B. anthracis* cell lysates with different dilutions of Eno serum. The antibodies recognize a ~45-kDa molecular-mass protein corresponding to Eno. Eno purified from *E. coli* was taken as a positive control, and GSH *S*-transferase was used as a negative control. Anti-PA antibody was used from the previous studies (41). For estimating protein size, prestained protein markers were used (Bio-Rad, catalog numbers 26616, 26619, and 26634).

Quantification and statistical analysis

For the radioactivity-based experiments, the autoradiograms were quantified using QuantityOne software (Bio-Rad), and the corresponding Coomassie Brilliant Blue–stained gels were quantified using Fiji-ImageJ. The normalized values were plotted using GraphPad Prism. The Western blots were quantified using Fiji-ImageJ software, and the respective values normalized by the controls were plotted using GraphPad Prism. For time-dependent 2D gel electrophoresis, the amount of phosphorylation at a given time point was calculated using the following formula.

Intensity of phosphorylation (at a given time point)

$$= \text{(Intensity of phosphoisoforms/Intensity of the total input protein)} \times 100 \quad \text{(Eq. 2)}$$

For statistical significance, a parametric unpaired *t* test was performed with Welch's correction.

Circular dichroism spectroscopy

CD spectra of Eno and its mutants (Eno-wt, Eno-UP, Eno-P, Eno$^{S336A/T363A/S367A}$) were recorded using a Jasco J-815 CD spectropolarimeter. The spectrum was recorded from 190 to 250 nm at 25 °C using a cell of 0.1-cm path length. Experiments were repeated thrice, and molar ellipticity values with respect to wavelength were analyzed using the K2D3 web server to estimate the protein secondary structure (48).

Animal ethics approval

The animal experiments were performed according to the Institutional Animal Ethics Committee (IAEC) of Defense Research and Development Establishment (registration number 37/GO/c/1999/CPCSEA dated April 13, 2011). The animals were maintained according to the approved guidelines of the Committee for the Purpose of Control and Supervision of Experiments on Animals (CPCSEA), Government of India. The study was also approved by the Institutional Biosafety Committee of Defense Research and Development Establishment (DRDO), Ministry of Defense, Government of India (protocol number IBSC/12/BT/AKG/22). For generation of antibodies, animals (mice and rabbits) were used after approval of the Animal Ethics Committee of CSIR–Institute of Genomics and Integrative Biology.

References

1. Arora, G., Misra, R., and Sajid, A. (2017) Model systems for pulmonary infectious diseases: paradigms of anthrax and tuberculosis. *Curr. Top. Med. Chem.* **17,** 2077–2099 CrossRef Medline
2. Beyer, W., and Turnbull, P. C. (2009) Anthrax in animals. *Mol. Aspects Med.* **30,** 481–489 CrossRef Medline
3. Errington, J. (2003) Regulation of endospore formation in *Bacillus subtilis*. *Nat. Rev. Microbiol.* **1,** 117–126 CrossRef Medline
4. Zheng, L., Abhyankar, W., Ouwerling, N., Dekker, H. L., van Veen, H., van der Wel, N. N., Roseboom, W., de Koning, L. J., Brul, S., and de Koster, C. G. (2016) *Bacillus subtilis* spore inner membrane proteome. *J. Proteome Res.* **15,** 585–594 CrossRef Medline
5. Sinai, L., Rosenberg, A., Smith, Y., Segev, E., and Ben-Yehuda, S. (2015) The molecular timeline of a reviving bacterial spore. *Mol. Cell* **57,** 695–707 CrossRef Medline
6. Segev, E., Smith, Y., and Ben-Yehuda, S. (2012) RNA dynamics in aging bacterial spores. *Cell* **148,** 139–149 CrossRef Medline
7. Mutlu, A., Trauth, S., Ziesack, M., Nagler, K., Bergeest, J. P., Rohr, K., Becker, N., Höfer, T., and Bischofs, I. B. (2018) Phenotypic memory in *Bacillus subtilis* links dormancy entry and exit by a spore quantity-quality tradeoff. *Nat. Commun.* **9,** 69 CrossRef Medline
8. Kuijper, B., and Johnstone, R. A. (2016) Parental effects and the evolution of phenotypic memory. *J. Evol. Biol.* **29,** 265–276 CrossRef Medline
9. Wang, S., Faeder, J. R., Setlow, P., and Li, Y. Q. (2015) Memory of germinant stimuli in bacterial spores. *MBio* **6,** e01859-15 CrossRef Medline
10. Pereira, S. F., Gonzalez, R. L., Jr, and Dworkin, J. (2015) Protein synthesis during cellular quiescence is inhibited by phosphorylation of a translational elongation factor. *Proc. Natl. Acad. Sci. U.S.A.* **112,** E3274–E3281 CrossRef Medline
11. Setlow, P. (2014) Germination of spores of *Bacillus species*: what we know and do not know. *J. Bacteriol.* **196,** 1297–1305 CrossRef Medline
12. Shah, I. M., Laaberki, M. H., Popham, D. L., and Dworkin, J. (2008) A eukaryotic-like Ser/Thr kinase signals bacteria to exit dormancy in response to peptidoglycan fragments. *Cell* **135,** 486–496 CrossRef Medline
13. Korza, G., Setlow, B., Rao, L., Li, Q., and Setlow, P. (2016) Changes in *Bacillus* spore small molecules, rRNA, germination, and outgrowth after extended sublethal exposure to various temperatures: evidence that protein synthesis is not essential for spore germination. *J. Bacteriol.* **198,** 3254–3264 CrossRef Medline

14. Commichau, F. M., Rothe, F. M., Herzberg, C., Wagner, E., Hellwig, D., Lehnik-Habrink, M., Hammer, E., Völker, U., and Stülke, J. (2009) Novel activities of glycolytic enzymes in *Bacillus subtilis*: interactions with essential proteins involved in mRNA processing. *Mol. Cell. Proteomics* **8,** 1350–1360 CrossRef Medline

15. Ghosh, S., Korza, G., Maciejewski, M., and Setlow, P. (2015) Analysis of metabolism in dormant spores of *Bacillus* species by ^{31}P nuclear magnetic resonance analysis of low-molecular-weight compounds. *J. Bacteriol.* **197,** 992–1001 CrossRef Medline

16. Sunde, E. P., Setlow, P., Hederstedt, L., and Halle, B. (2009) The physical state of water in bacterial spores. *Proc. Natl. Acad. Sci. U.S.A.* **106,** 19334–19339 CrossRef Medline

17. Leyva-Vazquez, M. A., and Setlow, P. (1994) Cloning and nucleotide sequences of the genes encoding triose phosphate isomerase, phosphoglycerate mutase, and enolase from *Bacillus subtilis*. *J. Bacteriol.* **176,** 3903–3910 CrossRef Medline

18. Setlow, P., and Kornberg, A. (1970) Biochemical studies of bacterial sporulation and germination. XXII. Energy metabolism in early stages of germination of *Bacillus megaterium* spores. *J. Biol. Chem.* **245,** 3637–3644 Medline

19. Agarwal, S., Kulshreshtha, P., Bambah Mukku, D., and Bhatnagar, R. (2008) α-Enolase binds to human plasminogen on the surface of *Bacillus anthracis*. *Biochim. Biophys. Acta* **1784,** 986–994 CrossRef Medline

20. Kudva, I. T., Griffin, R. W., Garren, J. M., Calderwood, S. B., and John, M. (2005) Identification of a protein subset of the anthrax spore immunome in humans immunized with the anthrax vaccine adsorbed preparation. *Infect. Immun.* **73,** 5685–5696 CrossRef Medline

21. Sajid, A., Arora, G., Singhal, A., Kalia, V. C., and Singh, Y. (2015) Protein phosphatases of pathogenic bacteria: role in physiology and virulence. *Annu. Rev. Microbiol.* **69,** 527–547 CrossRef Medline

22. Bryant-Hudson, K. M., Shakir, S. M., and Ballard, J. D. (2011) Autoregulatory characteristics of a *Bacillus anthracis* serine/threonine kinase. *J. Bacteriol.* **193,** 1833–1842 CrossRef Medline

23. Pompeo, F., Foulquier, E., and Galinier, A. (2016) Impact of serine/threonine protein kinases on the regulation of sporulation in *Bacillus subtilis*. *Front. Microbiol.* **7,** 568 CrossRef Medline

24. Setlow, P. (2008) Dormant spores receive an unexpected wake-up call. *Cell* **135,** 410–412 CrossRef Medline

25. Arora, G., Sajid, A., Arulanandh, M. D., Singhal, A., Mattoo, A. R., Pomerantsev, A. P., Leppla, S. H., Maiti, S., and Singh, Y. (2012) Unveiling the novel dual specificity protein kinases in *Bacillus anthracis*: identification of the first prokaryotic dual specificity tyrosine phosphorylation-regulated kinase (DYRK)-like kinase. *J. Biol. Chem.* **287,** 26749–26763 CrossRef Medline

26. Arora, G., Sajid, A., Gupta, M., Bhaduri, A., Kumar, P., Basu-Modak, S., and Singh, Y. (2010) Understanding the role of PknJ in *Mycobacterium tuberculosis*: biochemical characterization and identification of novel substrate pyruvate kinase A. *PLoS One* **5,** e10772 CrossRef Medline

27. Rosenberg, A., Soufi, B., Ravikumar, V., Soares, N. C., Krug, K., Smith, Y., Macek, B., and Ben-Yehuda, S. (2015) Phosphoproteome dynamics mediate revival of bacterial spores. *BMC Biol.* **13,** 76 CrossRef Medline

28. Arora, G., Sajid, A., Virmani, R., Singhal, A., Kumar, C. M. S., Dhasmana, N., Khanna, T., Maji, A., Misra, R., Molle, V., Becher, D., Gerth, U., Mande, S. C., and Singh, Y. (2017) Ser/Thr protein kinase PrkC-mediated regulation of GroEL is critical for biofilm formation in *Bacillus anthracis*. *NPJ Biofilms Microbiomes* **3,** 7 CrossRef Medline

29. Newman, J. A., Hewitt, L., Rodrigues, C., Solovyova, A. S., Harwood, C. R., and Lewis, R. J. (2012) Dissection of the network of interactions that links RNA processing with glycolysis in the *Bacillus subtilis* degradosome. *J. Mol. Biol.* **416,** 121–136 CrossRef Medline

30. Schreier, B., and Höcker, B. (2010) Engineering the enolase magnesium II binding site: implications for its evolution. *Biochemistry* **49,** 7582–7589 CrossRef Medline

31. Boël, G., Pichereau, V., Mijakovic, I., Mazé, A., Poncet, S., Gillet, S., Giard, J. C., Hartke, A., Auffray, Y., and Deutscher, J. (2004) Is 2-phosphoglycerate-dependent automodification of bacterial enolases implicated in their export? *J. Mol. Biol.* **337,** 485–496 CrossRef Medline

32. Leggett, M. J., McDonnell, G., Denyer, S. P., Setlow, P., and Maillard, J. Y. (2012) Bacterial spore structures and their protective role in biocide resistance. *J. Appl. Microbiol.* **113,** 485–498 CrossRef Medline

33. Granger, A. C., Gaidamakova, E. K., Matrosova, V. Y., Daly, M. J., and Setlow, P. (2011) Effects of Mn and Fe levels on *Bacillus subtilis* spore resistance and effects of Mn^{2+}, other divalent cations, orthophosphate, and dipicolinic acid on protein resistance to ionizing radiation. *Appl. Environ. Microbiol.* **77,** 32–40 CrossRef Medline

34. Lebioda, L., and Stec, B. (1991) Mechanism of enolase: the crystal structure of enolase-Mg^{2+}-2-phosphoglycerate/phosphoenolpyruvate complex at 2.2-Å resolution. *Biochemistry* **30,** 2817–2822 CrossRef Medline

35. Gao, X., Tang, Y., Rong, W., Zhang, X., Zhao, W., and Zi, Y. (2011) Analysis of binding interaction between captopril and human serum albumin. *Am. J. Anal. Chem.* **2,** 250–257 CrossRef

36. Shakir, S. M., Bryant, K. M., Larabee, J. L., Hamm, E. E., Lovchik, J., Lyons, C. R., and Ballard, J. D. (2010) Regulatory interactions of a virulence-associated serine/threonine phosphatase-kinase pair in *Bacillus anthracis*. *J. Bacteriol.* **192,** 400–409 CrossRef Medline

37. Yang, C. K., Zhang, X. Z., Lu, C. D., and Tai, P. C. (2014) An internal hydrophobic helical domain of *Bacillus subtilis* enolase is essential but not sufficient as a non-cleavable signal for its secretion. *Biochem. Biophys. Res. Commun.* **446,** 901–905 CrossRef Medline

38. Yang, C. K., Ewis, H. E., Zhang, X., Lu, C. D., Hu, H. J., Pan, Y., Abdelal, A. T., and Tai, P. C. (2011) Nonclassical protein secretion by *Bacillus subtilis* in the stationary phase is not due to cell lysis. *J. Bacteriol.* **193,** 5607–5615 CrossRef Medline

39. Singhal, A., Arora, G., Virmani, R., Kundu, P., Khanna, T., Sajid, A., Misra, R., Joshi, J., Yadav, V., Samanta, S., Saini, N., Pandey, A. K., Visweswariah, S. S., Hentschker, C., Becher, D., *et al.* (2015) Systematic analysis of mycobacterial acylation reveals first example of acylation-mediated regulation of enzyme activity of a bacterial phosphatase. *J. Biol. Chem.* **290,** 26218–26234 CrossRef Medline

40. Arora, G., Sajid, A., Arulanandh, M. D., Misra, R., Singhal, A., Kumar, S., Singh, L. K., Mattoo, A. R., Raj, R., Maiti, S., Basu-Modak, S., and Singh, Y. (2013) Zinc regulates the activity of kinase-phosphatase pair (BasPrkC/BasPrpC) in *Bacillus anthracis*. *Biometals* **26,** 715–730 CrossRef Medline

41. Singh, L. K., Dhasmana, N., Sajid, A., Kumar, P., Bhaduri, A., Bharadwaj, M., Gandotra, S., Kalia, V. C., Das, T. K., Goel, A. K., Pomerantsev, A. P., Misra, R., Gerth, U., Leppla, S. H., and Singh, Y. (2015) *clpC* operon regulates cell architecture and sporulation in *Bacillus anthracis*. *Environ. Microbiol.* **17,** 855–865 CrossRef Medline

42. Dale, J. L., Raynor, M. J., Ty, M. C., Hadjifrangiskou, M., and Koehler, T. M. (2018) A Dual role for the *Bacillus anthracis* master virulence regulator AtxA: control of sporulation and anthrax toxin production. *Front. Microbiol.* **9,** 482 CrossRef Medline

43. Paidhungat, M., and Setlow, P. (2000) Role of Ger proteins in nutrient and nonnutrient triggering of spore germination in *Bacillus subtilis*. *J. Bacteriol.* **182,** 2513–2519 CrossRef Medline

44. Singhal, A., Arora, G., Sajid, A., Maji, A., Bhat, A., Virmani, R., Upadhyay, S., Nandicoori, V. K., Sengupta, S., and Singh, Y. (2013) Regulation of homocysteine metabolism by *Mycobacterium tuberculosis* S-adenosylhomocysteine hydrolase. *Sci. Rep.* **3,** 2264 CrossRef Medline

45. Schmidl, S. R., Gronau, K., Pietack, N., Hecker, M., Becher, D., and Stülke, J. (2010) The phosphoproteome of the minimal bacterium *Mycoplasma pneumoniae*: analysis of the complete known Ser/Thr kinome suggests the existence of novel kinases. *Mol. Cell. Proteomics* **9,** 1228–1242 CrossRef Medline

46. Melo, R. C., Morgan, E., Monahan-Earley, R., Dvorak, A. M., and Weller, P. F. (2014) Pre-embedding immunogold labeling to optimize protein localization at subcellular compartments and membrane microdomains of leukocytes. *Nat. Protoc.* **9,** 2382–2394 CrossRef Medline

47. Arora, G., Sajid, A., Singhal, A., Joshi, J., Virmani, R., Gupta, M., Verma, N., Maji, A., Misra, R., Baronian, G., Pandey, A. K., Molle, V., and Singh, Y. (2014) Identification of Ser/Thr kinase and forkhead associated domains in *Mycobacterium ulcerans*: characterization of novel association between protein kinase Q and MupFHA. *PLoS Negl. Trop. Dis.* **8,** e3315 CrossRef Medline

48. Louis-Jeune, C., Andrade-Navarro, M. A., and Perez-Iratxeta, C. (2012) Prediction of protein secondary structure from circular dichroism using theoretically derived spectra. *Proteins* **80,** 374–381 CrossRef Medline